Buckling optimization of Double-Double (DD) laminates with gradual thickness tapering

Dan Wang [1,*], Zhoucheng Su [1], Sridhar Narayanaswamy [1], Stephen WL Tsai [2]

Abstract:

Double-double (DD) laminates are promising replacements for conventional Quad laminates in aerospace applications because of their inherent design simplicity and, more importantly, the ease of tapering. However, the thickness thinning due to tapering will significantly increase the risk of buckling failure. In this paper, we proposed an implicit global & local model for thickness tapering optimization of DD laminates to maximize buckling resistance under the given weight constraint or weight reduction under buckling constraints. Firstly, a global model is established for buckling load calculation, with material properties calculated from homogenization of local laminates using the classical laminate theory. Then, nodal repeats of a four-plies DD sub-laminate are chosen as design variables to interpolate the tapered thickness profile. Sensitivities of structural responses are calculated semi-analytically to achieve efficient gradient-based optimization. Tapering spacing constraints between adjacent thicknesses are introduced to mitigate the potential delamination due to the stress concentrations caused by sharp thickness variation at the cost of a reduced optimization effect. Finally, typical numerical examples show that DD laminates with optimal gradual thickness tapering can remarkably increase the structural buckling resistance or the weight reduction.

Key words: Double-double (DD) laminates; Thickness tapering; Buckling; Structural optimization; Spacing constraints

* Corresponding author, wangd@ihpc.a-star.edu.sg

1 Institute of High Performance Computing (IHPC), Agency for Science, Technology and Research (A*STAR), 1 Fusionopolis Way, #16-16 Connexis, 138632, Republic of Singapore

2 Department of Aeronautics & Astronautics, Stanford University, Durand Building, 496 Lomita Mall, Stanford, CA 94305-4035, United States

1. Introduction

Composite structures have been widely used in aerospace engineering due to their high strength-to-weight ratio. The conventional way of stacking up laminate composites is to adopt plies with 0, 90 and ±45 degree angles with different sequences, which is the so-called Quad layups. The original concern of just using 0, 90 and ±45 degree plies is due to the deficiency of equipment or devices to accurately locate plies with an arbitrary angle. With the development and mature of automated prepreg layup technology and advanced inspection system [1-3], this restraint should be broken. However, the Quad layups are still in a dominant position for both research and industry applications. The optimal layups and the thickness tapering are usually achieved by varying, deleting, or adding the candidate plies through zero-order algorithms, like genetic algorithms (GA) [4], ant colony algorithms [5], Harmony search algorithms [6, 7], and permutation search algorithms [8, 9], due to the discrete nature of Quad layups. Some researchers also have adopted a free-angle layup and try to find the optimal ply orientations using similar optimization methods [10, 11].

For both Quad and free angle laminate design, if constraints are not suitably included in the design, the obtained optimal layups may not be realistic. This is mainly due to two reasons: 1) multiple layers of the same angle stacking together unable to resist secondary loading or other failure modes; 2) optimized layups with completely different ply orientations for all plies make the manufacturing expensive and challenging. For example, the optimal layups of $[0_4]_s$ [10], $[90_{12}]$ [12], and $[0_{10}]_s$ [13] are obtained if the number of repeated layers is not restricted, which will lead to delamination and thereby destroy the optimization effect. Moreover, layups of $[-87.2^o/35.9^o/47.0^o/69.1^o/32.7^o/-57.5^o/-36.5^o/-54.2^o/-49.8^o/-44.2^o]$ [11] for free angle design and $[-45^o_4/-90^o/-45^o_3/-90^o_3/-45^o_3/0^o/-45^o/-90^o_2/-45^o_3/0^o/45^o_4/90^o/45^o_3/90^o_3/45^o_3/0^o/45^o/90^o_2/45^o_3/0^o]_s$ from Quad design [14] may pose great manufacturing challenges. When the free ply orientation variation is combined with suitable guidelines, efficient and reliable layups are produced. Le-Manh et. al. [14] proposed the layup of $[\theta_1/\theta_2]_s$ and $[\theta_1/\theta_2/\theta_3/\theta_4]_s$ with symmetric constraints and used GA to optimize the maximum buckling resistance of a rectangular plate. It was found that

[±45]$_s$ has the largest buckling resistance for a square panel under uniaxial or biaxial compression or shear [15]. Javidrad et. al. [16] also proposed three different layups of [±θ], [90/±θ], and [0/±θ] with θ varying with steps of 15°. Zhang et al. [17] proposed four different ply stacking sequences of [±θ]$_{10}$, [±θ/±θ/±10/±θ/±θ]$_2$, [±θ/±10/±θ/±10/±θ]$_2$, and [±10/±θ/±10/±θ/±10]$_2$ for maximum specific energy absorption of a circular tube.

Double-Double (DD) laminates, proposed by Tsai [15,18,19], adopting two pairs of balanced ply orientations as thin-assembly building blocks, as illustrated in Fig. 1, revolutionize the limitations imposed by conventional Quad layups and preserve the most important guidelines, in the most concise and efficient way. At the same time, DD laminate can be fabricated as thin-assembly building blocks to achieve 4 to 8 times speed over Quad for the same tape width using one axis layup and tapering with multi-axial tapes, which are commercially available as Chomarat Non-Crimp Fabric (NCF) laminates [15,18]. The unique feature of DD leads to easy thickness tapering by taking advantage of thin ply and repeatable sub-laminate, which is significant in achieving light-weight laminate structural design for aerospace applications. Kappel at DLR fabricated a tapered DD spar with a 41.5% weight saving compared with uniform design [20, 21]. Moreover, DD laminates can achieve the equivalent 10% rule for secondary loading resistance in the conventional Quad with the layup of [Φ/-ψ/-Φ/ψ]$_r$ by adding constraints on ply angles and differences between two independent angles.

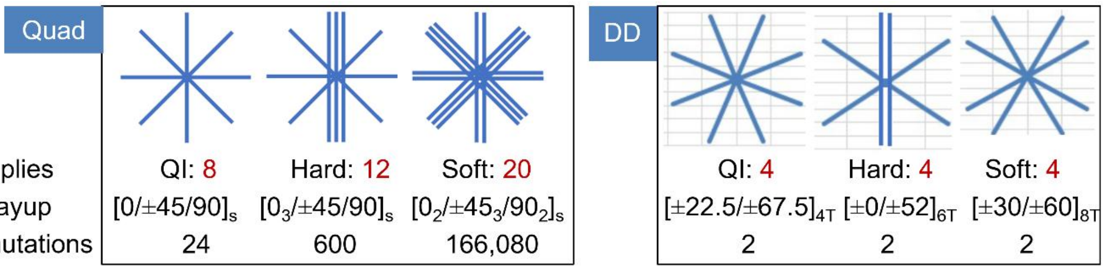

Figure 1 Simplicity of DD laminates compared with matched Quad stiffness. [21]

The biggest advantages of DD laminates are to simplify the tapering process with homogenized material properties and provide a continuous field by varying DD angles to control the structural performance, which is difference from the discrete field of Quad laminates by adding or deleting plies in the thickness direction. It is noticeable that buckling performance is very critical for DD laminates due to the remarkably increased buckling risk with the thickness thinning in tapering. Thus, integrating the buckling consideration into the design and optimization procedure is crucial for a successful industry adoption of DD.

If the same ply stacking sequences and/or the same thickness are applied to the whole laminate in the optimization process, the structural stiffness will keep constant, which is the so-called constant stiffness (CS) design, that covers most of previous ply orientation and laminate stacking sequences optimization. On the contrary, the stiffness can be varied by optimizing curved fiber path [22-31], thickness tapering [32-39], or using curved stiffeners as reinforcements [40-42], which together can be treated as variable stiffness (VS) design. Shape [43, 44] and topology optimization [45, 46] of the overall material distribution can also realize in-plane stiffness variation for composite structures but is normally classified as separate optimization problems.

The optimization problems for thickness tapering of composite laminates are normally solved as laminate bending using stacking sequence tables of discrete ply orientations to decide the ply drop sequences based on zero-order evolutionary algorithms [32-36]. It is also possible to adopt gradient-based algorithms to determine the thickness distribution first and then to finalize the ply drop sequences [37, 38]. When the set of stacking sequences is fixed, a level-set method can be used to optimize the thickness distribution of composite structures with a conventional Quad layup [39]. Design guidelines for manufacturing-oriented ply-drop [47, 48] and novel scarf tapering strategies [49, 50] have been proposed to reduce the stress concentration due to thickness variation. Besides, the development of manufacturing techniques, such as laser-assisted tape placement (LATP) together with relevant research work [51] helps to accelerate the industry adoption of tapered composite structures by mitigating the defects in manufacturing.

In this work, we propose an implicit global & local homogenized model to perform thickness tapering optimization for DD laminates for maximizing buckling resistance under a weight constraint or weight reduction under buckling constraints. Modeling and parameterization strategies for thickness variations are provided in Section 2. Mathematical optimization models incorporating tapering spacing constraints between adjacent thicknesses are defined in Section 3 together with the involved sensitivity calculation and optimization procedure. After that, typical numerical examples including a benchmark problem with an 18-panel horseshoe configuration, a hole-free square and a perforated square under four different loading cases, and a C-spar under multiple gradually reduced vertical loads are provided in Section 4 to demonstrate the effectiveness of the proposed optimization method. Finally, the conclusions are given in Section 5.

2. Modelling and parameterization of DD laminates with thickness tapering

DD is a novel laminate layup as a repeat of the sub-laminate made up of two groups of balanced ply orientations, as illustrated in Fig. 1. For DD laminates, the layup of $[\Phi/\text{-}\psi/\text{-}\Phi/\psi]_r$ is selected as the best among the possible stacking sequences since its strength-bending coupling, i.e. B matrix, is the smallest [15, 21], which will help to maintain the flat shapes after curing even symmetry is abandoned in DD laminates. In that case, the out-of-plane stiffness matrix ends up to the same as the in-plane stiffness matrix after normalization.

From the perspective of structural optimization, DD can provide better results naturally by expanding the design space largely with tailored thickness tapering. Due to the simplicity with the same normalized in-plane and out-of-plane stiffness, one whole structure made up of DD laminates can be treated as using one material, like metals, and only need to emphasis on the thickness variation to achieve the best performance. This is also the main reason why the proposed highly efficient gradient-based optimization method can be used in DD laminates, but not in the conventional Quad laminates.

The key technologies of modelling strategy and parameterization strategies for thickness tapering of DD laminates will be discussed in this section.

2.1. Implicit global & local modelling strategy

An implicit global & local modelling strategy is used here to evaluate the buckling resistance of the DD laminate with thickness variation. Shell elements without explicit thickness information are used to model the global laminate panel. Material properties for different elements of the global model are assigned based on the homogenization calculation of the local models with detailed thickness tapering information. As illustrated in Fig. 2, the proposed implicit global/local modelling techniques are in analogy to those used in our previous work for curved grid stiffener path design [40-42]. Unlike the explicit homogenization in curved grid design, the homogenization process of the local models is implicitly achieved by assigning different layups or equivalent material properties, which is underlyingly solved using the closed form equations from the classical laminate theory without explicitly establishing the finite element models of the local cell configurations.

(a) Detailed tapering model (b) Global & local tapering model

Figure 2. Implicit global & local model for DD laminates with thickness tapering.

2.2. Design parameterization of thickness tapering using streamline functions

To obtain the best DD laminates, thickness profiles of DD laminates vary with the number of sub-laminate repeats to obtain the optimal thickness distribution. Here, the numbers of repeats for the selected DD sub-laminate at different locations are selected as design variables. The real thickness equals to the thickness of four plies multiplying with the number of sub-laminate repeats. Design variables can be defined on elements to form a discrete thickness distribution, as illustrated in Fig. 3(a), or on mesh nodes to form a continuous thickness distribution by interpolation, as illustrated in Fig. 3(b). When design variables are associated to elements, the discrete thickness distribution provides no correlation among adjacent elements. On the contrary, when design variables are associated to nodes, continuous thickness contours can be formed by sharing the same values at the common nodes and interpolating adjacent nodal values to obtain elemental values, as illustrated in Fig. 3(b). Therefore, it is better to associate design variables to nodes rather than elements for a clearer tapered boundaries by forming a strong coupling of thickness variations in adjacent elements.

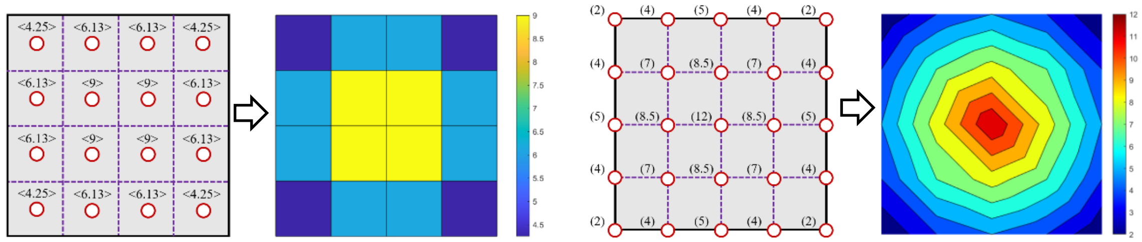

(a) Elemental definition (b) Nodal definition

Figure 3. Distribution of the repeat number for a DD sub-laminate representing the tapered thickness distribution on a discrete mesh associated to elements or nodes.

Thus, the nodal distribution of the repeat number of the selected DD sub-laminate are used to control the thickness variation. It is necessary to point out that in the simulation, the repeat numbers of a DD sub-laminate are firstly assigned to the nodes of a discrete mesh (Fig. 3(b) left). Then the values on the elements can be calculated based on interpolation of the related nodal values. These nodal and elemental values are not required to be integers, they are continuous values depending on how the optimizer returns the updated design variables for a better solution. Noticeably, the simulation model with each element having different repeat numbers of sub-laminates is different from the illustration of the structure with interpolated repeat numbers (Fig. 3(b) right). When the number of elements is large enough and the repeat numbers of a DD sub-laminate are rounded to be integers, the simulation model will approach to the accurate tapered structure.

In Fig. 4, it is assumed that the same value of repeats is treated as located on the same contour line with the expression of:

$$\varphi(x, y) = c \tag{1}$$

Suppose another point in the neighborhood lies on the adjacent contour line with the expression of:

$$\varphi(x+\Delta x, y+\Delta y) = c+1 \tag{2}$$

By applying the Taylor expression to the left of Eq. (2), it is obtained that:

$$\varphi(x+\Delta x, y+\Delta y) = \varphi(x,y) + \Delta x\frac{\partial\varphi(x,y)}{\partial x} + \Delta y\frac{\partial\varphi(x,y)}{\partial y} + O((\Delta x,\Delta y)^2) \tag{3}$$

Subtracting Eq.(1) from Eq.(3), and ignoring higher order terms, yields the following expression:

$$\{\Delta x, \Delta y\}\boldsymbol{\nabla}\varphi = 1 \tag{4}$$

As shown in Fig. 4, the tapering spacing of adjacent thicknesses can be calculated as the distance of adjacent repeats of the DD sub-laminate, which is the projection of points on adjacent contour lines onto their normal, with the expression of:

$$s = \{\Delta x, \Delta y\}\frac{\boldsymbol{\nabla}\varphi}{\|\boldsymbol{\nabla}\varphi\|} = \frac{\mathbf{1}}{\|\boldsymbol{\nabla}\varphi\|} \tag{5}$$

The repeat number of a DD sub-laminate associated to an element can be interpolated from those of its adjacent nodes, but not the reverse. For instance, the elemental distribution shown in Fig. 3(a) results from interpolation from the nodal distribution depicted in Fig. 3(b). The interpolation formulation is:

$$r_e = \sum_{i=1}^{n^{\{e\}}} N_i^{\{e\}}\,\varphi_{i^{\{e\}}} \tag{6}$$

where the subscript e and the superscript $\{e\}$ denote quantities for the e-th element, and the subscript i denote those of the i-th node in the element; r and φ are the repetition numbers of the sub-laminate on elements and nodes, respectively; n and N are the node number and its shape functions associated to one element, respectively. Noticeably, $i^{\{e\}}$ and $N_i^{\{e\}}$ denotes the node number of the i-th node for the e-th element.

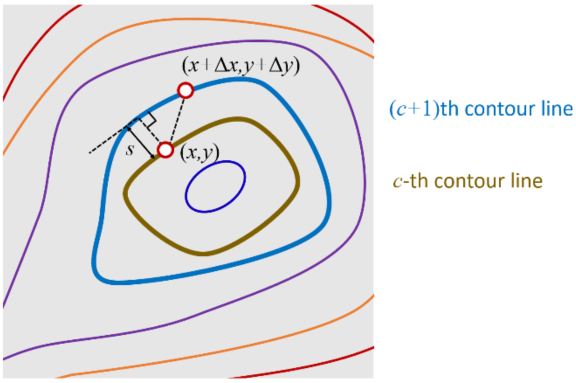

Figure 4. Schematic illustration of the tapering spacing between adjacent thickness using the repeat number of a DD sub-laminate defined by contour lines.

3. Optimization of DD laminates with gradual thickness tapering

Given the large number of design variables associated to finite element nodes, it is essential to adopt gradient-based algorithms for efficient optimization. DD laminates with 4-plies building blocks are used here because their constant normalized stiffness, similar to metals, enables the use of gradient-based algorithms. In contrast, conventional Quad laminates with single ply drops exhibit varying normalized stiffness, resulting in a discrete stiffness distribution unsuitable for gradient-based algorithms. Additionally, if Quad laminates drop one sub-laminate like DD, the tapering thickness becomes too thick due to the symmetric requirement and the nature of adding or deleting plies for stiffness variation with fixed ply angles.

Two different optimization models incorporating the tapering spacing constraints are introduced here to achieve gradual thickness tapering of DD laminates for maximum weight reduction or buckling resistance. Then, sensitivity analysis is carried out for the involved structural responses and spacing constraints. Finally, the optimization procedure is provided, summarizing the implementation steps and the key techniques used.

3.1. Optimization model of tapered DD laminates with tapering spacing constraints

As explained in Section 2, design variables are associated to the mesh nodes instead of the elements, which are physically defined as the repeat number of a selected DD sub-laminate. Multiplying the design variables with the thickness of one sub-laminate will provide the real laminate thickness. Although the repeats should be integers for physical meanings, continuously varying values are used here for the convenience of integration with high-efficient gradient-based algorithms. This is achievable based on two facts: 1) the simplicity of DD laminates with the same in-plane and out-of-plane stiffness after normalization using the best stacking sequence of [Φ/-ψ/-Φ/ψ]; 2) the homogenized material properties with thickness variation, as metals, following four-plies drop together.

The optimal thickness distribution with tapering profiles can largely increase the critical buckling load of DD laminates with the same material usage. However, the lumped thickness distribution may bring material failure forward due to potential delamination between adjacent thickness variations. The stress concentration at the ply drop position may seriously reduce the optimization effect. As experimentally verified in the Damghani's work [52], the "optimal" structure may lead to earlier bucking deformation and lower post-buckling failure load.

To solve this problem, we incorporate tapering spacing constraints into the optimization procedure and use the minimum tapering spacing between adjacent thicknesses to improve the load distribution and mitigate the potential of delamination due to stress concentration. It is noticed that one sub-laminate with four plies at the same ply drop location is used to achieve the same normalized stiffness for the whole structure. Thus, thin plies are preferred for DD laminates to on one hand make a fast fabrication using multi-axial tapes, and on the other hand to reduce the stress concentration due to four ply drops at the same location.

Here, two mathematical optimization models of DD laminates are utilized for achieving gradually tapered thickness profiles: 1) for minimizing the structural weight with buckling load constraints; 2) for maximizing the critical buckling load with the structural weight constraint, which correspond to Eqs. (7) and (8), respectively.

$$\begin{cases} \text{Find: } \mathbf{x} = [\varphi_1, \quad \varphi_2, \quad \cdots, \quad \varphi_n] \\ \text{Min: } W \\ \qquad s.t. \;\; \chi_i = \dfrac{1}{\lambda_i} \leq 1 \,, \quad i = 1,2,\dots,m \\ \qquad s_k \geq s_L, \quad k = 1,2,\dots,n_e \\ \qquad \mathbf{x} - \overline{\mathbf{x}} \leq \mathbf{0} \\ \qquad \underline{\mathbf{x}} - \mathbf{x} \leq \mathbf{0} \end{cases} \tag{7}$$

$$\begin{cases} \text{Find: } \mathbf{x} = [\varphi_1, \quad \varphi_2, \quad \cdots, \quad \varphi_n] \\ \text{Min: } \max\left(\chi_i = \dfrac{1}{\lambda_i}\right), \quad i = 1,2,\dots,m \\ \; s.t. \quad V \leq V_0 \\ \qquad\quad s_k \geq s_L, \quad k = 1,2,\dots,n_e \\ \qquad\quad \mathbf{x} - \overline{\mathbf{x}} \leq \mathbf{0} \\ \qquad\quad \underline{\mathbf{x}} - \mathbf{x} \leq \mathbf{0} \end{cases} \tag{8}$$

where $\mathbf{x}$ denotes design variables as the repeat number of the selected DD sub-laminate at different nodes, with $\underline{\mathbf{x}}$ and $\overline{\mathbf{x}}$ as its lower and upper bounds; φ_j is the j-th component of $\mathbf{x}$; χ_i is the reciprocal of the i-th buckling load λ_i, which is used to create a minimum objective function or a negative constraint; V and V_0 are the structural volume and its upper bound, respectively; s_k is the tapering spacing of the adjacent thicknesses associated to elements and bounded by the lower bound of s_L.

In the implementation, the problem of minimizing the maximum value of Eq. (8) is transformed into a minimization problem by introducing an artificial design variable z. Consequently, the optimization model is rewritten as:

$$\begin{cases} \text{Find: } \mathbf{x} = [\varphi_1, \quad \varphi_2, \quad \cdots, \quad \varphi_n, \quad z] \\ \text{Min: } z \\ s.t. \;\; g_{\lambda_i} = \dfrac{1}{\lambda_i} - z \leq 0, \quad i = 1,2,\dots,\mathrm{m} \\ \qquad g_V = V - V_0 \leq 0 \\ \qquad g_{s_k^2} = (\boldsymbol{\nabla} r_k)^2 - \dfrac{1}{s_L^2} \leq 0, \quad k = 1,2,\dots,n_{\mathrm{E}} \\ \qquad \mathbf{g}_{\overline{\mathbf{x}}} = \mathbf{x} - \overline{\mathbf{x}} \leq \mathbf{0} \\ \qquad \mathbf{g}_{\underline{\mathbf{x}}} = \underline{\mathbf{x}} - \mathbf{x} \leq \mathbf{0} \end{cases} \tag{9}$$

Here one type of constraints is added: an upper bound constraint for the reciprocal of the buckling loads. Noticeably, this upper bound z also works as an artificial design variable and the design objective for solving the problem of minimizing the maximum. Besides, a square version of the spacing constraints is used to simplify the sensitivity calculation, which is calculated using Eq. (5) in analogy to the calculation used in our previous work of the stiffener spacing for curved grid-stiffener layout optimization [40-42]. The formulation is expressed as:

$$(\nabla r_k)^2 = \mathbf{b}_k^T \mathbf{L}_k \mathbf{b}_k \tag{10}$$

where $\mathbf{b}_k = \left[\varphi_{1^{\{k\}}}, \varphi_{2^{\{k\}}}, \dots, \varphi_{n^{\{k\}}}\right]^T$ denotes the nodal design variables of the k-th element with $n^{\{k\}}$ representing the number of nodes in this element with the superscript $\{k\}$ representing the quantities of the k-th element. $\mathbf{L}_k$ is the Laplace matrix representing the dot product of the gradients of shape functions relating to the k-th element, with the expression of:

$$\mathbf{L}_k = \frac{1}{A_k}\int_{\Omega_k} \nabla\mathbf{N}^{\{k\}} \cdot \nabla\mathbf{N}^{\{k\}} d\Omega_k \tag{11}$$

where $\mathbf{N}$ denotes shape functions, and A_k is the elemental area of the domain Ω_k. The superscript $\{k\}$ and the subscript k all denotes the quantities of the k-th element.

It is noticeable that there are three possible failure modes implicitly considered in the above optimization models. The lower bound of the repeat number of sub-laminates will help to avoid local buckling modes and local material failure when the local thicknesses are too thin. The thickness tapering spacing constraints are added to avoid potential delamination due to stress concentration caused by sharp thickness variations.

3.2. Sensitivity analysis

Design variable associated to a simulation mesh for finite element calculation, or a background mesh should be mapped back to the simulation mesh. In both cases, the number of design variables is large for the sake of having a good control of the overall thickness distribution. Thus, Lam Search [15, 21] based on listing is not sufficient to deal with general thickness tapering optimization. Instead, advanced gradient-based structural optimization techniques requiring sensitivity calculation are needed for calculation efficiency.

Sensitivity with respect to design variables is carried out using the chain rule:

$$\frac{\partial f}{\partial \mathbf{x}} = \sum_{e=1}^{n_{\mathrm{E}}} \frac{\partial f}{\partial \mathbf{C}_e} \frac{\partial \mathbf{C}_e}{\partial r_e} \frac{\partial r_e}{\partial \mathbf{x}} \tag{12}$$

The last item in the above equation is obtained by deriving Eq. (6):

$$\frac{\partial r_e}{\partial \varphi_{i\{e\}}} = N_i^{\{e\}} \tag{13}$$

where $i^{\{e\}}$ is the number of the i-th node of the e-th element, and $\varphi_{i\{e\}}$ is the repeat number of the sub-laminate on this node, which is one of the design variables.

The second component in the right part of Eq. (12) is calculated as:

$$\frac{\partial \mathbf{C}_e}{\partial r_e} = \frac{1}{r_e} \begin{bmatrix} \mathbf{A}_e & \mathbf{0} \\ \mathbf{0} & 3\mathbf{D}_e \end{bmatrix} \tag{14}$$

by driving the following components of $\mathbf{C}_e$ with respect to the elemental repeat of the sub-laminate:

$$\mathbf{A}_e = t\widetilde{\mathbf{A}}_0 = r_e t_0 \widetilde{\mathbf{A}}_0 = r_e \mathbf{A}_0 \tag{15}$$

$$\mathbf{D}_e = t^3 \widetilde{\mathbf{A}}_0 = r_e^3 t_0^3 \widetilde{\mathbf{A}}_0 = r_e^3 \mathbf{D}_0 \tag{16}$$

where $\widetilde{\mathbf{A}}_0$ and $\mathbf{A}_0$ are the membrane stiffness matrices for a unit thickness and the thickness of one sub-laminate denoting by t_0, respectively, and the formal matrix is also known as normalized material stiffness matrix. $\mathbf{D}_0$ is the bending stiffness matrix for one sub-laminate. Both $\mathbf{A}_0$ and $\mathbf{D}_0$ are independent of r_e.

Now, the only unknown component in the right part of Eq. (12) is the first item representing the sensitivity with respect to the equivalent material stiffness, which is provided below, and the detailed derivation equations are available in the reference [40].

3.2.1 Sensitivity of the reciprocal buckling load

As shown in Eqs. (7) and (8), the reciprocal values of the buckling loads are used in order to achieve a minimum objective or a negative constraint. The sensitivity is expressed as:

$$\frac{\partial \chi_i}{\partial \mathbf{C}_e} = \frac{\partial \left(\frac{1}{\lambda_i}\right)}{\partial \mathbf{C}_e} = -\frac{1}{\lambda_i^2}\frac{\partial \lambda_e}{\partial \mathbf{C}_e} \tag{17}$$

The buckling load is calculated based on the following equation [40]:

$$(\mathbf{K} - \lambda \mathbf{K}^G)\mathbf{a} = 0 \tag{18}$$

where **K** and **K**^{G} denote the structural tangent and geometric stiffness matrices, respectively. **a** is the deformation vector representing the buckling mode and λ is the buckling load factor based on the applied load. The buckling mode is normally normalized to satisfy:

$$\mathbf{a}^T \mathbf{K} \mathbf{a} = 1 \tag{19}$$

Thus, the derivative of Eq. (18) is multiplied by **a**^{T} to the left to get the following formulation:

$$(\mathbf{a}^T \mathbf{K}^G \mathbf{a}) \frac{\partial \lambda_e}{\partial \mathbf{C}_e} = \mathbf{a}^T \left(\frac{\partial \mathbf{K}}{\partial \mathbf{C}_e} - \lambda \frac{\partial \mathbf{K}^G}{\partial \mathbf{C}_e}\right) \mathbf{a} \tag{20}$$

where

$$\mathbf{a}^T \mathbf{K}^G \mathbf{a} = \frac{1}{\lambda} \mathbf{a}^T \mathbf{K} \mathbf{a} = \frac{1}{\lambda} \tag{21}$$

By substituting Eq. (21) into (20), it is obtained that:

$$\frac{\partial \lambda_e}{\partial \mathbf{C}_e} = \lambda \mathbf{a}^T \left(\frac{\partial \mathbf{K}}{\partial \mathbf{C}_e} - \lambda \frac{\partial \mathbf{K}^G}{\partial \mathbf{C}_e}\right) \mathbf{a} \tag{22}$$

In Eq. (22), the first unknown item is the derivative of the stiffness matrix with respect to the equivalent material stiffness, whose component is calculated as:

$$\frac{\partial \mathbf{K}}{\partial (\mathbf{C}_e)_{ij}} = \frac{\partial \mathbf{K}_e}{\partial (\mathbf{C}_e)_{ij}} = \frac{1}{2}\int_{\Omega} \left((\mathbf{B}_e)_{i:}^T(\mathbf{B}_e)_{j:} + (\mathbf{B}_e)_{j:}^T(\mathbf{B}_e)_{i:}\right) d\Omega \tag{23}$$

with $\mathbf{B}_e$ is the elemental strain-displacement matrix for the *e*-th element.

The geometric stiffness matrix is calculated using the following formulation:

$$\mathbf{K}_e^G = -\mathbf{R}_e\mathbf{G}_e \tag{24}$$

where $\mathbf{R}_e$ is the elemental stress resultants with the components of $\{\mathbf{R}_e^x, \mathbf{R}_e^y, \mathbf{R}_e^{xy}\}$ for two compressions and one shear; $\mathbf{G}_e$ is a combination of three constant matrices $\{\mathbf{G}_e^x, \mathbf{G}_e^y, \mathbf{G}_e^{xy}\}$, which are only related to the elemental geometry. The formulation of $\mathbf{R}_e$ is expressed as:

$$\mathbf{R}_e = \mathbf{C}_e\boldsymbol{\varepsilon}_e = \mathbf{C}_e\mathbf{B}_e\mathbf{u}_e \tag{25}$$

with $\boldsymbol{\varepsilon}_e$ and $\mathbf{u}_e$ are the elemental strain and displacement vectors.

Thus, the second unknown item in Eq. (22) is calculated as:

$$\frac{\partial \mathbf{K}^G}{\partial \mathbf{C}_e} = -\sum_{e=1}^{n_\mathrm{E}} \frac{\partial \mathbf{R}_e}{\partial \mathbf{C}_e}\mathbf{G}_e \tag{26}$$

with the derivative of the stress resultants expressed as:

$$\frac{\partial \mathbf{R}_e}{\partial \mathbf{C}_e} = \boldsymbol{\varepsilon}_e + \mathbf{C}_e\mathbf{B}_e\frac{\partial \mathbf{u}_e}{\partial \mathbf{C}_e} = \boldsymbol{\varepsilon}_e + \mathbf{C}_e\mathbf{B}_e\mathbf{L}_e\frac{\partial \mathbf{u}}{\partial \mathbf{C}_e} \tag{27}$$

where $\mathbf{L}_e$ is the index matrix for the local displacement vector.

The last unknown item in Eq. (27) is the derivative of the displacement with respect to the equivalent material stiffness, which is calculated by taking derivative of the equilibrium equation and ends up to an adjoint problem of:

$$\mathbf{K}\frac{\partial \mathbf{u}}{\partial \mathbf{C}_e} = -\frac{\partial \mathbf{K}}{\partial \mathbf{C}_e}\mathbf{u} \tag{28}$$

At this point, the sensitivity of the buckling load to the equivalent material stiffness is solved, together with the sensitivity of the reciprocal buckling load from Eq. (12).

3.2.2 Sensitivity of the structural volume

The structural volume is expressed as:

$$V=\sum_{e=1}^{n_{\mathrm{E}}} A_e r_e t_0 \tag{29}$$

where A_e and r_e are the elemental area and the repeat number with respect to one sub-laminate for the e-th element. t_0 is the thickness of one sub-laminate. Thus, its sensitivity is calculated as:

$$\frac{\partial V}{\partial \mathbf{x}}=\frac{\partial V}{\partial r_e}\frac{\partial r_e}{\partial \mathbf{x}}=A_e t_0 \frac{\partial r_e}{\partial \mathbf{x}} \tag{30}$$

with the last item in the above equation is expressed in Eq. (13).

3.2.3 Sensitivity of the tapering spacing constraints

The sensitivity of the tapering spacing constraints of Eq. (10) is expressed as:

$$\frac{\partial g_{s_k}}{\partial \varphi_j}=2\nabla r_k \frac{\partial(\nabla r_k)}{\partial \varphi_j}=4\nabla r_k \mathbf{L}_k \mathbf{b}_k \frac{\partial \mathbf{b}_k}{\partial \varphi_j} \tag{31}$$

where φ_j is the repeat number for the sub-laminate for the j-th node. The last item of the right part of Eq. (31) is non-zero only when $i^{\{k\}}=j$.

3.3. Optimization procedure

The optimization procedure is provided in Fig. 5, including three key technologies: 1) implicit global & local modeling strategy, 2) design parameterization, and 3) simulation and sensitivity calculation of a tapered DD laminates with gradual thickness variation. The first two aspects have been explained in Section 2 and the last one aspect is provided in Section 3.

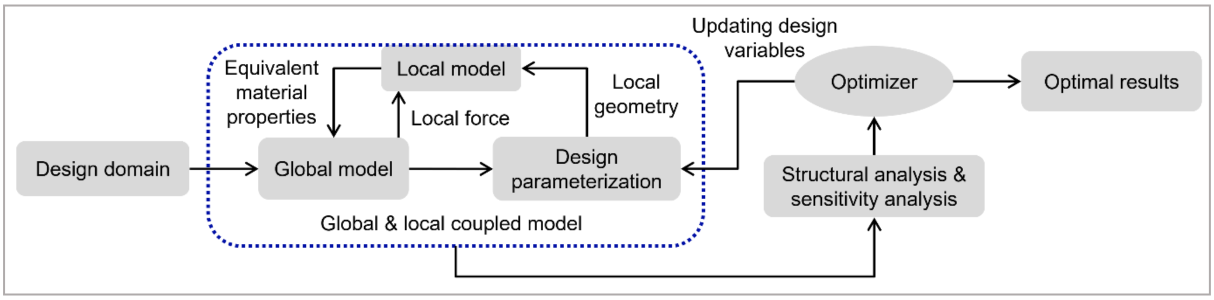

Figure 5. Optimization procedure for varying thicknesses of DD laminates with thickness tapering.

The details of a similar optimization procedure can be found in curved grid-stiffener design using streamline stiffener path optimization [40]. A globally convergent optimization algorithm for successive convex approximations is used here as the optimizer [53].

4. Numerical examples

Four numerical examples are used to validate the effectiveness of the proposed method: 1) an 18-panel horseshoe configuration; 2) a hole-free square panel; 3) a square panel with a central hole; and 4) a C-spar. Two different optimization models of Eqs. (7) and (8) are used to minimize the structural weight with buckling constraints and maximize the critical buckling load with weight constraint, respectively. The 1st example is a benchmark problem for weight reduction using Eq. (7) from literature [33, 34, 54, 55] for validation. The 2nd and 3rd examples are for buckling increase using Eq. (8) to explore the influence of cutout and different loads on the optimal tapering solution. The last example of a C-spar for buckling increase is used to represent an industry application under non-uniformly distributed load. In 2nd to 4th examples, the structural weight is constrained to be the same as that with uniform seven repeats of the sub-laminate.

For the 1st example, composite material of IM7/8552 is used with the properties of E_1=141 GPa, E_2=9.03 GPa, G_{12}=4.27 GPa, v_{12}=0.32, ρ= 1.574 g/cm^3. For the 2nd to 4rd examples, composite material of IM7/977 is used with the properties of E_1=191 GPa, E_2=9.94 GPa, G_{12}=7.79 GPa, and v_{12}=0.35. A DD laminate with a thin ply thickness of 0.0625 mm and a layup of $[58^\circ/-32^\circ/-58^\circ/32^\circ]_r$ is adopted here, which is a soft laminate with an equivalent stiffness as the conventional Quad layup of $[\pm45^\circ_2/90^\circ/\pm45^\circ_2/0^\circ]_s$.

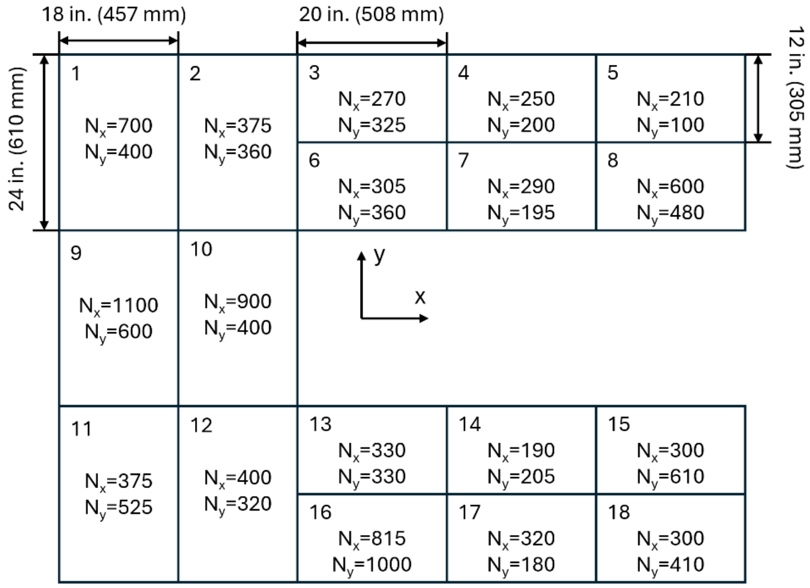

Figure 6. Geometry and loading constraints of an 18-panel horseshoe configuration [33].

4.1. A benchmark problem with an 18-panel horseshoe configuration

As illustrated in Fig. 6, an 18-panel horseshoe configuration are used here as a benchmark problem for comparison with literature [33, 34, 53, 54]. Each panel is simply supported and compressed biaxially with the loads labeled.

4.1.1 Optimal results based on local buckling constraints

The benchmark problem from literature is based on optimization of minimizing the structural weight with local buckling constraints of the 18 panels. Here, a soft DD laminate layup of $[58^\circ/-32^\circ/-58^\circ/32^\circ]_r$ is used to investigate the optimal results of using the proposed method, where *r* is the repeat number of the sub-laminate. The obtained optimal weight and buckling loads of each panel are provided in Table 1 together with three optimal solutions from literature. Meanwhile, optimal thickness profiles represented by the distribution of the repeats of the DD sub-laminate are provided in Fig. 7. It shows that using the proposed method can achieve a weight of 26.51 kg with the reduction of 1.58 kg compared with the best solution of 28.09 kg from literature [33]. By using gradual thickness variation, all the local buckling load constraints of each panel are active to reach the lower limit.

Table 1. Comparison of optimal laminate layups of the optimal 18-panel horseshoe configuration for local buckling resistance.

Panel	Literature solutions						Proposed solution	
	IJSSelmuiden [55]		Irisarri [34]		Yang [33]			
	n_{plies}	$\lambda_{\min}$	n_{plies}	$\lambda_{\min}$	n_{plies}	$\lambda_{\min}$	$n_{\text{plies}}^{\text{AVG}}$	$\lambda_{\min}$
1	34	1.114	34	1.166	33	1.056	30.9	1.000
2	30	1.173	28	1.037	28	1.004	25.7	1.000
3	22	1.308	22	1.145	21	1.050	19.6	1.000
4	18	1.048	19	1.077	18	1.025	17.0	1.000
5	16	1.206	16	1.065	16	1.203	14.7	1.000
6	22	1.176	22	1.029	22	1.087	20.4	1.000
7	18	1.016	19	1.043	19	1.125	17.1	1.000
8	26	1.235	26	1.096	25	1.042	23.6	1.000
9	38	1.028	38	1.048	38	1.049	36.2	1.000
10	36	1.104	35	1.045	35	1.043	33.1	1.000
11	30	1.011	30	1.103	30	1.074	27.1	1.000
12	30	1.168	28	1.033	28	1.000	25.8	1.000
13	22	1.231	22	1.078	22	1.137	20.0	1.000
14	18	1.112	19	1.143	18	1.087	16.6	1.000
15	26	1.197	26	1.062	25	1.010	24.0	1.000
16	32	1.032	32	1.079	31	1.011	29.9	1.000
17	18	1.029	19	1.058	18	1.007	17.0	1.000
18	22	1.066	24	1.205	23	1.104	21.1	1.000
Weight (kg)	28.69		28.55		28.09		26.51	

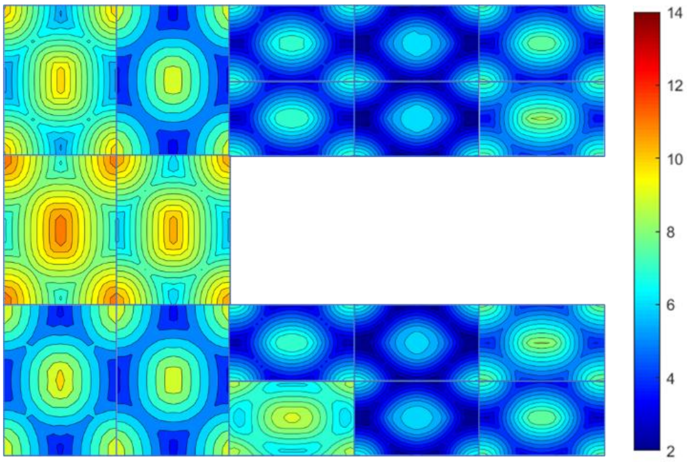

Figure 7. Optimal thickness profiles represented by the DD repeats for an 18-panel horseshoe configuration with soft stiffness to resist local buckling.

4.1.2 Optimal results based on global buckling constraints

The benchmark problem in Section 4.1.1 is executed based on two simplifications: 1) negligence of the load redistribution after updating the local thicknesses; 2) local buckling (Fig. 8(a)) dominates the failure mode and the structure will buckle following the partitioned local panels. In fact, it is very hard to satisfy these two assumptions when the horseshoe configuration is treated as one whole structure. As illustrated in Fig. 8(b), the horseshoe panel under biaxial compression with N_x=N_y=5977.5 N will buckle at global mode. Thus, the global buckling constrained problem is also investigated here and three different DD laminate layups of [58°/-32°/-58°/32°]$_r$, [68°/-22°/-68°/22°]$_r$ and [50°/0°/-50°/0°]$_r$ are used in the optimization corresponding to soft, Quasi-Isotropic (QI) and hard stiffness, respectively, to investigate the influence of laminate layups.

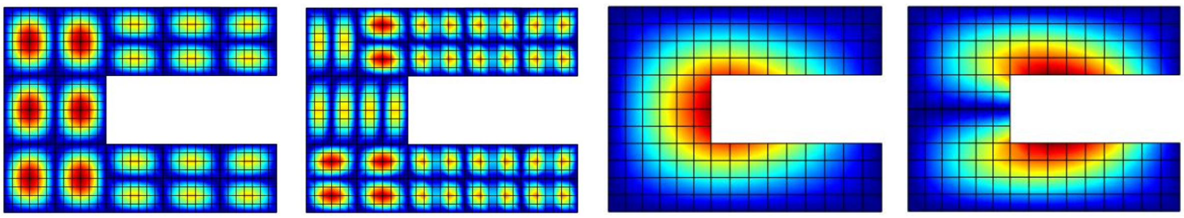

Mode 1 Mode 2 Mode 1 Mode 2

(a) Local buckling in Section 4.1.1 (b) Global buckling in Section 4.1.2

Figure 8. Buckling modes of the horseshoe structure.

Optimal thickness distributions and performances of horseshoe structures for global buckling resistance are provided in Fig. 9 and Table 2, respectively, for three typical stiffness. The optimal thickness profiles are similar for three stiffness with the material more located at four corners and the vertical cutout edge. 29% to 19% weight reductions are achieved compared with an initial uniform laminate with 32 layers (i.e. 8 repeats). For an initial 28 layers soft laminate, almost the same weight reduction of 19.8% is achieved by optimization as the hard laminate with an initial 32 layers. In both cases, the buckling constraint of the first mode is active in the initial design achieves, while the buckling constraints of the first two modes are both active in the optimal design.

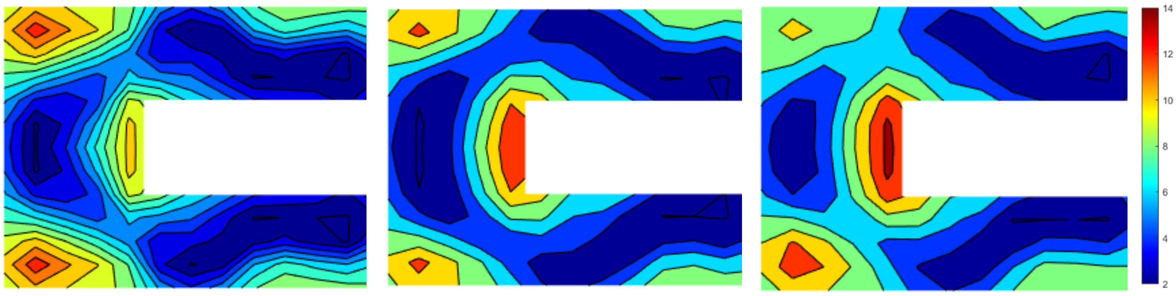

(a) Soft: [58°/-32°/-58°/32°]$_r$ (b) QI: [68°/-22°/-68°/22°]$_r$ (c) Hard: [50°/0°/-50°/0°]$_r$

Figure 9. Optimal thickness profiles represented by the DD repeats for an 18-panel horseshoe configuration to resist global buckling.

Table 2 Comparison of the weight and critical buckling load of the optimal 18-panel horseshoe configuration for global buckling resistance.

Stiffness	Initial uniform thickness			Optimal tapered thickness			Weight reduction
	W (kg)	λ_1	λ_2	W (kg)	λ_1	λ_2	
Soft	29.717	1.001	2.027	23.843	1.000	1.000	19.8%
	33.963	1.496	3.027	24.002	1.000	1.000	29.3%
QI	33.963	1.275	2.930	24.571	1.000	1.000	27.6%
Hard	33.963	1.001	2.336	27.351	1.000	1.000	19.4%

4.2. A hole-free square panel

As illustrated in Fig. 10, four loading cases are considered: uniaxial compression, biaxial compression, positive shear, and negative shear for a hole-free 300 mm*300mm square panel with simply supported boundary conditions. The spacing constraints are set to be 31.75 mm as 127 times of one sub-laminate thickness of 0.25 mm in this example. The first three loading cases are used to do optimization separately as a single loading case, while a multiple loading case of both positive shear and negative shear together is included for the fourth optimization to explore the tapering profile for the largest buckling resistance under dual shears.

The process for dual shears optimization is realized by including negative buckling load factors in the eigenvalue calculation, and rewrite the optimization model of Eq. (8) as:

$$\begin{cases} \text{Find: } \mathbf{x} = [\varphi_1, \quad \varphi_2, \quad \cdots, \quad \varphi_n] \\ \text{Min: } \max\left(\chi_i^2 = \dfrac{1}{\lambda_i^2}\right), \quad i = 1,2,3 \\ s.t. \quad V \le V_0 \\ \qquad\quad s_k \ge s_L, \quad k = 1,2,\ldots,n_e \\ \qquad\quad \mathbf{x} - \overline{\mathbf{x}} \le \mathbf{0} \\ \qquad\quad \underline{\mathbf{x}} - \mathbf{x} \le \mathbf{0} \end{cases} \tag{32}$$

where the reciprocal of the square of the buckling load factor is used as the objective function to constrain both negative and positive buckling loads.

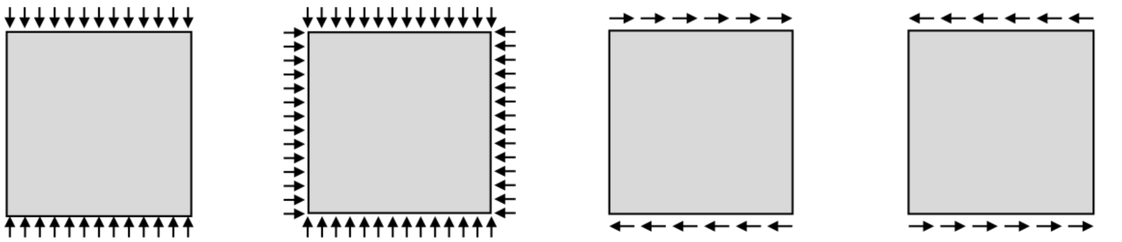

(a) Uniaxial compression (b) Biaxial compression (c) Positive shear (d) Negative shear

Figure 10. Different loading cases of a hole-free square panel.

To investigate the influence of spacing constraints, both optimal results for the model without and with spacing constraints are provided for comparison.

- **Without spacing constraints**

A performance comparison of the hole-free square with uniform thickness, and optimal tapered thickness is provided in Table 3. Optimal results show that the critical buckling loads can be increased by 53.0%, 79.2%, 76.3% and 29.0%, under uniaxial compression, biaxial compression, one shear, and dual shears, respectively, compared with a panel with a uniform thickness under the same structural weight. The increases are significant expect the dual shears case, which has a lower increase by coordinating dual shears along opposite directions.

Table 3. Performance comparison of a hole-free square panel with uniform thickness, and optimal tapered thickness under the same structural weight.

Loading type	Thickness profile	Spacing constraints	Buckling load factor				λ_1 increase by tapering
			λ_1	λ_2	λ_3	λ_4	
Uniaxial compression	Uniform	-	18.26	25.88	42.52	66.86	-
	Optimal	without	27.94	27.94	35.3	43.12	53.0%
		with	22.22	24.56	40.18	60.26	21.7%
Biaxial compression	Uniform	-	9.12	20.7	20.72	36.68	-
	Optimal	without	16.34	16.78	16.82	21.52	79.2%
		with	10.98	20.12	20.14	33.86	20.4%
One shear	Uniform	-	42.91	50.13	115.05	125.11	-
	Optimal	without	75.64	75.64	148.89	167.70	76.3%
		with	52.42	52.42	106.97	108.8	22.1%
Dual shears	Uniform		-42.86	42.86	-50.06	50.13	-
	Optimal	without	-55.30	55.30	-55.30	55.30	29.0%
		with	-53.01	53.01	-53.06	53.06	23.7%

Optimal thickness profiles for a hole-free square panel represented by the contour of sub-laminate repeats are illustrated in Fig. 11 for the optimization model without tapering spacing constraints.

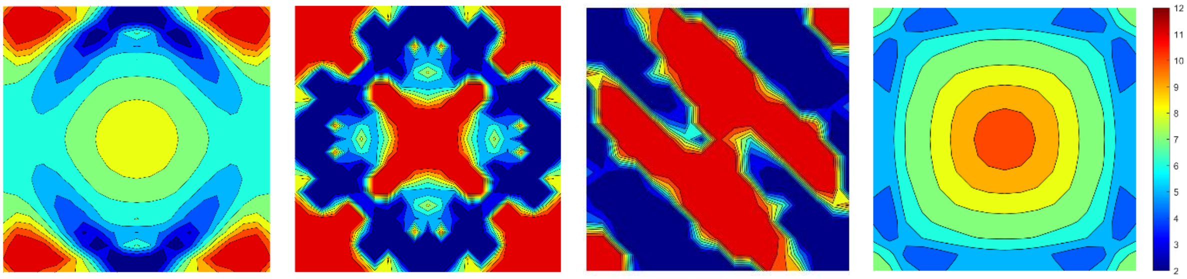

(a) Under uniaxial compression (b) Under biaxial compression (c) Under one shear (d) Under dual shears

Figure 11. Optimal thickness profiles for a hole-free square panel represented by the contour of the repeat number of a sub-laminate without tapering spacing constraints.

- **With spacing constraints**

Optimal thickness profiles incorporating the tapering spacing constraints of the hole-free square panel are illustrated in Fig. 12. It is shown that the repeat number of a sub-laminate gradually varies while maintaining the same largest material enhancements at the boundary corners and central most deformed area as the results in previous solutions, if the tapering spacing constraints are incorporated in the optimization. These gradually varied thickness profiles provide more reliable structures with higher strengths in composite laminate practice. This advantage is achieved at the cost of a largely reduced optimization effect. It is summarized in Table 3 that the buckling load increases will drop to 21.7%, 20.4%, 22.1% and 23.7% for four different loading cases, when the tapering spacing constraints are included.

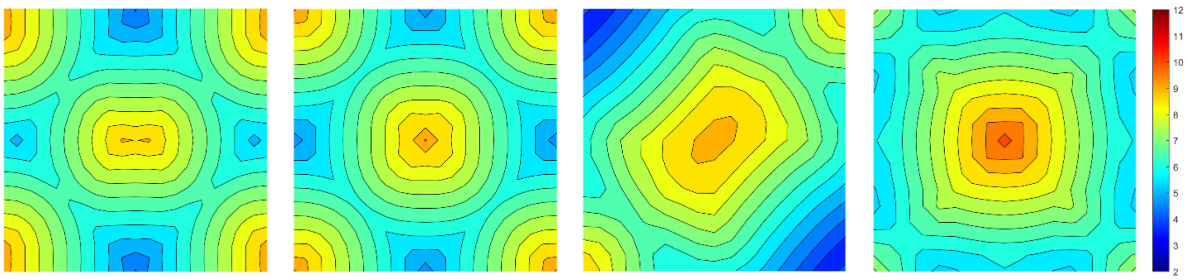

(a) Under uniaxial compression (b) Under biaxial compression (c) Under one shear (d) Under dual shear

Figure 12. Optimal thickness profiles for a hole-free square panel represented by the repeat contour with spacing constraints under different loading cases.

4.2.1 Discussion of optimal thickness profiles

The optimal thickness distributions in Fig. 11 without considering the tapering spacing constraints show that both the square corners and the central point, which correspond to the constrained points and the largest deformed point, respectively, are critical for enhancing the buckling resistance. Under uniaxial compression, the materials are almost uniformly distributed except the lumped boundary areas, while a ±45° enhancement is required and the material enhancement at four corners has interchangeable axis symmetry for the central area when biaxial compression is considered. Under one shear loading, the materials are lumped near the center area along the compressed direction, while an almost circle enhancement is required at that area when dual shears are considered to increase the buckling load for two different compressed directions. Moreover, it is noticeable that the optimal thickness profiles with materials lumped at critical regions are not practical for composite laminates due to the potential delamination caused by shape thickness variations.

When the thickness tapering spacing constraints are included in the optimization, the thickness distribution is similar for Fig. 11 and Fig. 12 if you compared the four corners and the center area. For the loading cases of uniaxial compression, biaxial compression, and dual shear, it is easy to interpret how the thicknesses of the lumped distribution in Fig. 11 are gradually tapered from the thickest area to the thinnest area to form a gradual thickness variation in Fig. 12. While for the loading case of one shear, the maximum thickness both occurs at the center and the left bottom and the right top corners with or without spacing constraints. In Fig. 11(c), it is clearly shown that besides the center and two corners, the maximum thickness also occurs at the compressed diagonal, while in Fig. 12(c) the required gradual transition from the center with maximum thickness to the top left and bottom right corners with the minimum thickness forms a thickness tapering contour distribution in circles of gradually increased approximate rectangles of similar shape. Noticeably, the compressed diagonal in the Fig. 12(c) still maintains high thickness.

4.2.2 Discussion of the iteration history and the calculation efficiency

Iteration histories of the tapering optimization process for a hole-free square panel under different loading cases are provided in Fig. 13. It is shown that all the optimizations converge within 50 iterations. In the optimization process, sub-problems are constructed at each iteration based on the values of required responses and their sensitivities. The simplest quadratic items of $\mathbf{x}^2$ are used to construct a convex subproblem with a tunable vector of coefficients, since the Hessian matrix is not calculated. When the tunable coefficients are big, the optimal solution of the sub-problem will be more conservative and easier to get stuck in a local optimal. So, in the optimization, small tunable coefficients are firstly given and then keep updated in each 10 iterations to help the optimization converge to an optimum. Then these coefficients will be reset to the initial small values in order to search for a better solution jumping out of the previous local optimum, which can be illustrated in Fig. 13 for the case under one shear loading without spacing constraints, with a big increase in the buckling load at 21th iteration.

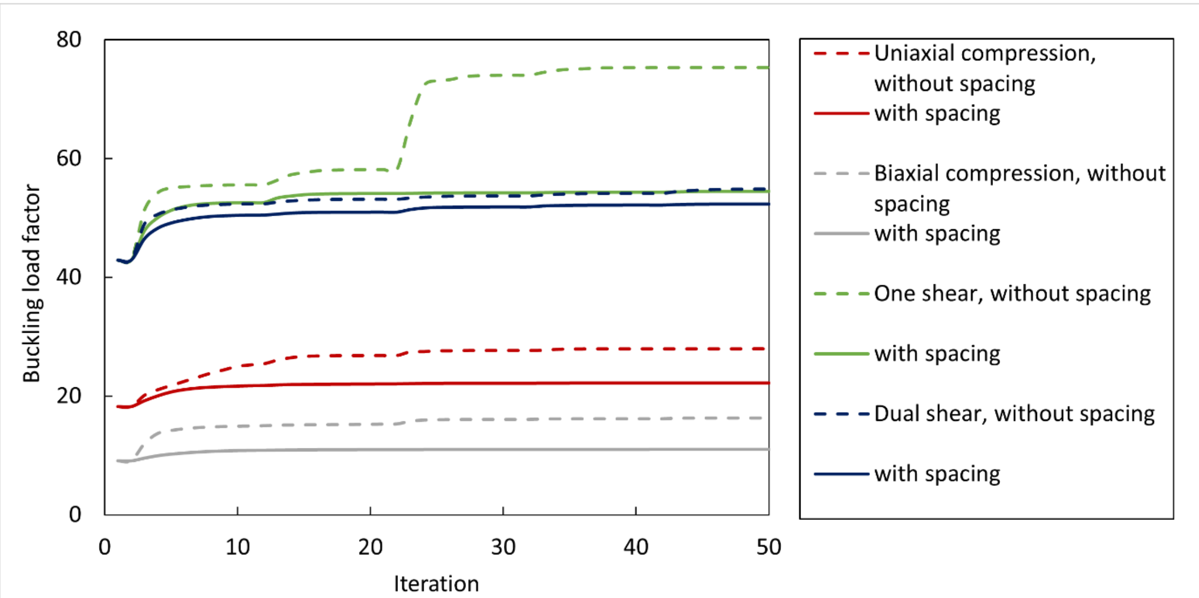

Figure 13. Iteration histories of the tapering optimization process for a hole-free square panel under different loading cases.

Here, the finite element (FE) simulation process is based on homogenized properties and the optimization process is based on gradient-based algorithm using adjoint semi-analytical sensitivities of Eq. (28), so the computational effort is low for each iteration, which is about three times of FE simulation time for one optimization iteration with one for FE simulation for calculating structural properties, one for solving the adjoint problem of Eq. (28) and one for other preprocessing and postprocessing. The FE simulation and optimization are all implemented in Matlab 2021 version using two cores of a mobile workstation. For this example, 52 mins, 68 mins, 60 mins and 74 mins are required for finishing the whole optimization procedure with 50 iterations for a mesh of 256 elements. So, it is about 0.42 mins to finish one FE simulation in that case and averagely, 63.6 mins are required to complete the whole optimization with 50 iterations using the proposed method.

To achieve an arbitrary thickness tapering profile, it is required to have a large number of design variables, similar as topology optimization. So, alternatives of using zero-order algorithms, which is commonly used in previous published work, are not affordable in time effort. If zero-order algorithms are used, a much longer time is required. For example, if Genetic Algorithm (GA) is used for this example with 81 independent design variables, each generation require 810 individuals, which means 810 independent FE simulations for one generation. At least 50 generations are required for the convergency of using GA. So, the total time required to complete one optimization process is 17,010 mins, equivalent to 11.8 days, based on 0.42 mins for one FE simulation and 40500 simulations in total. Using GA, the required time is about 267 times as that is required by using our proposed method.

Thus, the proposed method has the advantage of achieving arbitrary thickness tapering profile high efficiently with affordable time effort. Similar as topology optimization, the method is for conceptual design. Detailed design based on high-fidelity FE simulations is required for more accurate solutions. It is noticeable that if zero-order algorithms are used, detailed design is also required for further validation.

4.3. A square panel with a central hole

A square panel with a central hole is used here as another example to investigate the influence of cutout on the optimal thickness profiles. Like the example of hole-free laminates in Section 4.2, we also utilized four loading cases, as illustrated in Fig. 14.

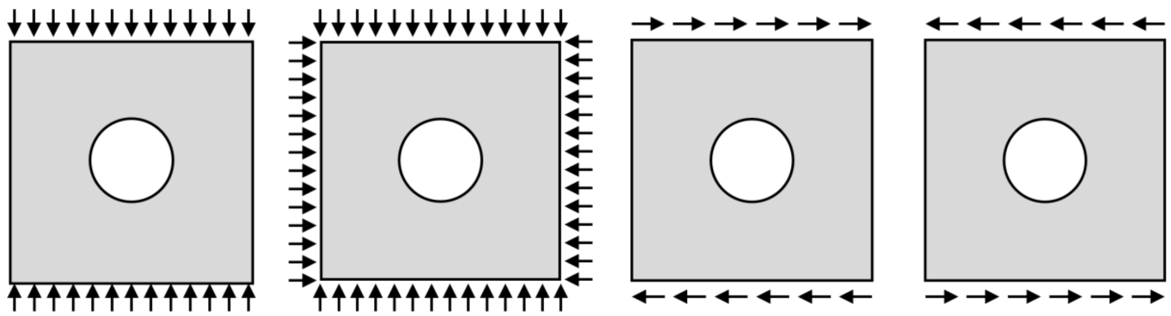

(a) Under uniaxial compression | (b) Under biaxial compression | (c) Under positive shear | (d) Under negative shear

Figure 14. Loading cases of a perforated square panel.

A performance comparison of the perforated square with uniform thickness, and optimal tapered thickness is provided in Table 4. Optimal thickness profiles are illustrated in Figs. 15 and 16 for the optimization model without and with tapering spacing constraints, respectively.

As summarized in Table 4, the critical buckling loads are increased by 69.8%, 70.8%, 129.9% and 87.2%, under four different loading cases, respectively, compared to that with a uniform thickness under the same structural weight. All the increases are significant if the spacing constraints are not included. The buckling load reduction due to the hole is evaluated by comparing it with the same item of the hole-free results in Table 1. Except the result under the biaxial compression, the perforated impact on the critical buckling load reduction is alleviated by using tapering, as shown in the grey shaded items in Table 4. However, this effect only validates for the one shear case when the tapering spacing constraints are added. As illustrated in Fig. 16(c), gradual thickness tapering can remarkably enhance the buckling resistance of the perforated panel under one shear by 63.2%, much larger than the improvements of panels under other loading cases ranging from 15.5% to 21.4%. At the same time, similar conclusions are obtained by comparing Figs. 15 and 16 that adding tapering spacing constraints can effectively control a gradual thickness variation of DD laminates ending up to favorable variation between adjacent thicknesses at the cost of a discounted optimization effect.

Table 4. Performance comparison of a perforated square with uniform thickness, and optimal tapered thickness under the same structural weight.

Loading type	Thickness profile	Spacing constraints	Buckling load factor				λ_1 reduce for hole	λ_1 increase by tapering
			λ_1	λ_2	λ_3	λ_4		
Uniaxial compression	Uniform	-	14.66	25.86	38.5	40.74	19.7%	-
	Optimal	without	24.90	24.90	34.00	45.66	10.9%	69.8%
		with	17.80	27.02	38.96	44.80	19.9%	21.4%
Biaxial compression	Uniform	-	7.47	17.64	17.67	27.92	18.1%	-
	Optimal	without	12.76	17.02	17.14	20.5	21.9%	70.8%
		with	8.63	18.38	18.40	26.56	21.4%	15.5%
One shear	Uniform	-	24.03	42.24	45.94	71.28	44.0%	-
	Optimal	without	55.24	55.27	89.07	99.11	27.0%	129.9%
		with	39.21	66.44	68.76	112.47	25.2%	63.2%
Dual shears	Uniform	-	24.03	-24.03	42.24	-42.24	43.9%	-
	Optimal	without	44.99	-44.99	-44.99	45.01	18.6%	87.2%

		with	28.79	-28.79	-50.25	50.29	45.7%	19.8%

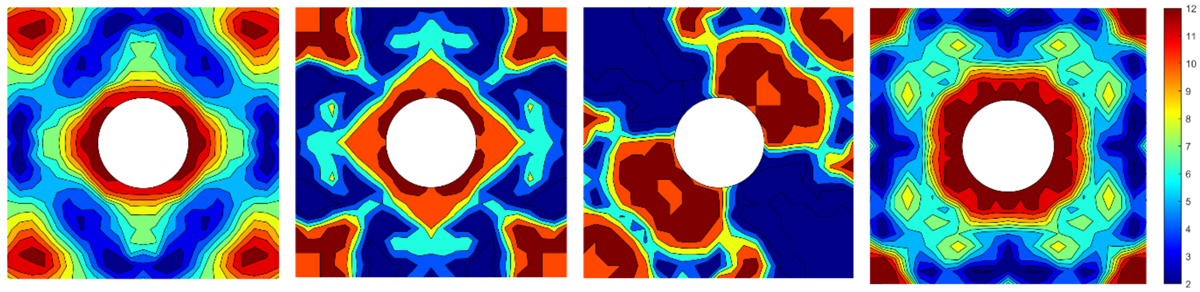

(a) Under uniaxial compression (b) Under biaxial compression (c) Under one shear (d) Under dual shears

Figure 15. Optimal thickness profiles for tapered DD laminates with a central hole.

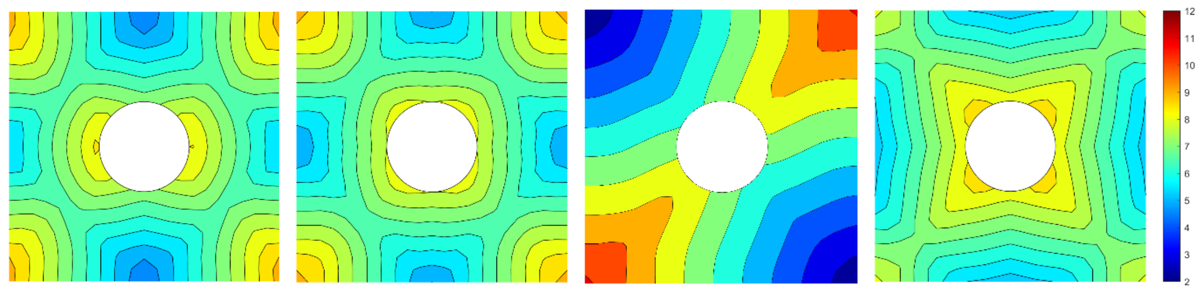

(a) Under uniaxial compression (b) Under biaxial compression (c) Under one shear (d) Under dual shears

Figure 16. Optimal thickness profiles for tapered DD laminates with a central hole including tapering spacing constraints.

4.4. A C-spar under multiple gradually reduced loading

A C-spar under multiple gradually reduced vertical loads is used here to investigate the effect of thickness tapering on buckling load improvement, to represent the wing spar for the potential application in aerospace industry. Loading, boundary conditions, and geometry of the C-spar structure are illustrated in Fig. 17. The structure is fixed at one side and a linearly reduced load from 2 kN to 0.5 kN along x direction, similar as the loading reduction from root to tip in wing structure, is applied on the C-spar at four uniformly distributed cross-sections along x direction. It is noticeable that, the loading is not just applied at the top surface of the

C-spar, but instead each loaded cross-section is assumed to be connected to an individual fixture, which will keep the whole loaded cross-section preserving the same displacement. The involved geometry parameters are given as follows: L=1 m, H=0.1 m, d=0.05 m.

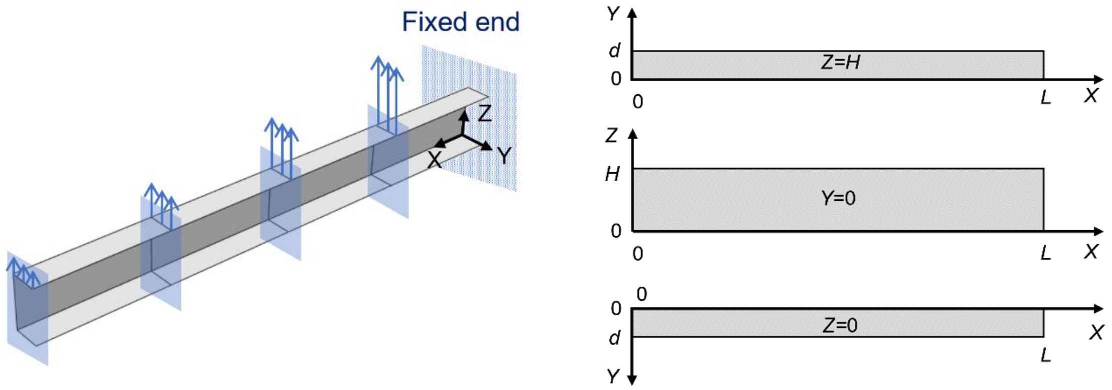

(a) Loading and boundary conditions (b) Geometry parameters

Figure 17. Schematic diagram of a C-spar structure made up of three panels.

When the gradually reduced loads are applied along z direction, the fixed end of the C-spar will bear the largest load and therefore should have the thickest design. Thus, thickness tapering should be effective in that case. Two different lowest spacings of 31.75 mm and 95.25 mm are set to investigate the influence of the size of tapering spacing on the optimal tapering results.

As provided in Table 5, the optimal tapering results of the C-spar are compared with that using the uniform thickness with seven repeats of the DD sub-laminate and that using a linearly distributed thickness tapering. All the designs preserve the same structural weight. When a general tapering profile with gradual thickness variation is used for optimization, as illustrated in Fig. 18(b) and (c), the critical buckling loads are increased remarkably by 394.1% and 281.5%, without and with spacing constraints of s_{min}=31.75 mm, respectively. In this example, the spacing constraints of s_{min}=31.75 mm is quite low compared to the length of 1000 mm of the C-spar. So, it might be challenging to manufacture the tapered laminates with a complicated thickness profile. Therefore, we triple the spacing constraints to s_{min}=95.25 mm to achieve a more manufacturing favorable tapering profile, as illustrated in Fig. 18(d). Here, the critical buckling load increase is reduced to 217.2% for enlarged tapering spacing constraints, however, which is still 77.7% higher than that using the optimal linear tapering, as illustrated in Fig. 18(a), on the buckling increase.

Table 5. Performance comparison of a C-spar with uniform thickness, linearly tapered thickness, and optimal tapering thickness under the same structural weight.

Thickness profile represented by DD sub-laminate repeats		Buckling load factor								λ_1 increase
		λ_1	λ_2	λ_3	λ_4	λ_5	λ_6	λ_7	λ_8	
Uniform (7 repeats)		2.38	3.22	4.42	4.69	5.36	5.58	6.51	7.02	0%
Linear tapering	From 12 to 2	1.05	2.48	3.53	3.89	4.16	4.50	4.96	5.25	-55.9%
	From 10 to 4	5.70	6.09	6.15	6.39	6.42	8.79	9.32	9.46	139.5%
Optimal tapering (mm)	No s_{min}	11.76	11.76	11.77	11.79	11.82	11.88	11.97	12.16	394.1%
	s_{min}=31.75	9.08	9.08	9.09	9.11	9.13	9.24	9.35	9.38	281.5%
	s_{min}=95.25	7.55	7.55	7.59	7.60	7.67	7.85	7.90	9.16	217.2%

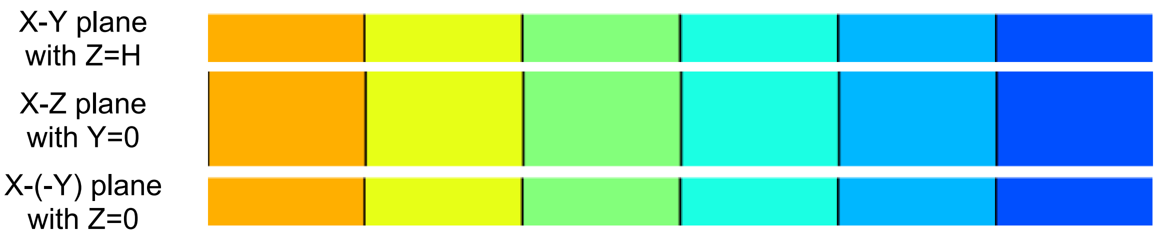

(a) Optimal linear tapering

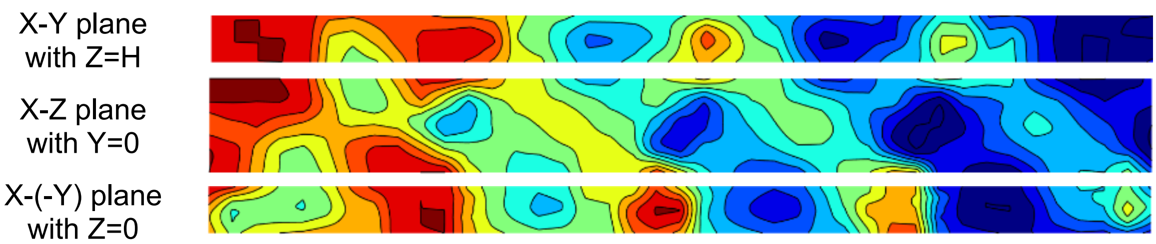

(b) Optimal tapering for the buckling resistance without spacing constraints

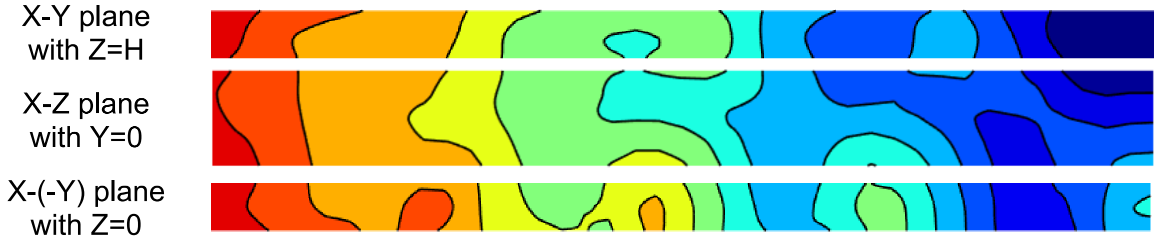

(c) Optimal tapering for the largest buckling resistance with spacing constraints of s_{min}=31.75 mm

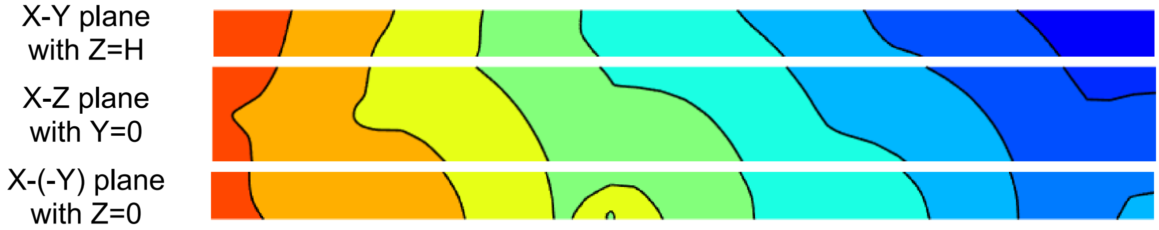

(d) Optimal tapering for the largest buckling resistance with spacing constraints of s_{min}=95.25 mm

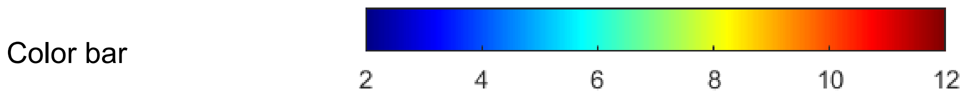

Figure 18. Distribution of the DD repeats for the optimal C-spars by unfolding the structure into the same plane from the three panels in Fig. 17(b).

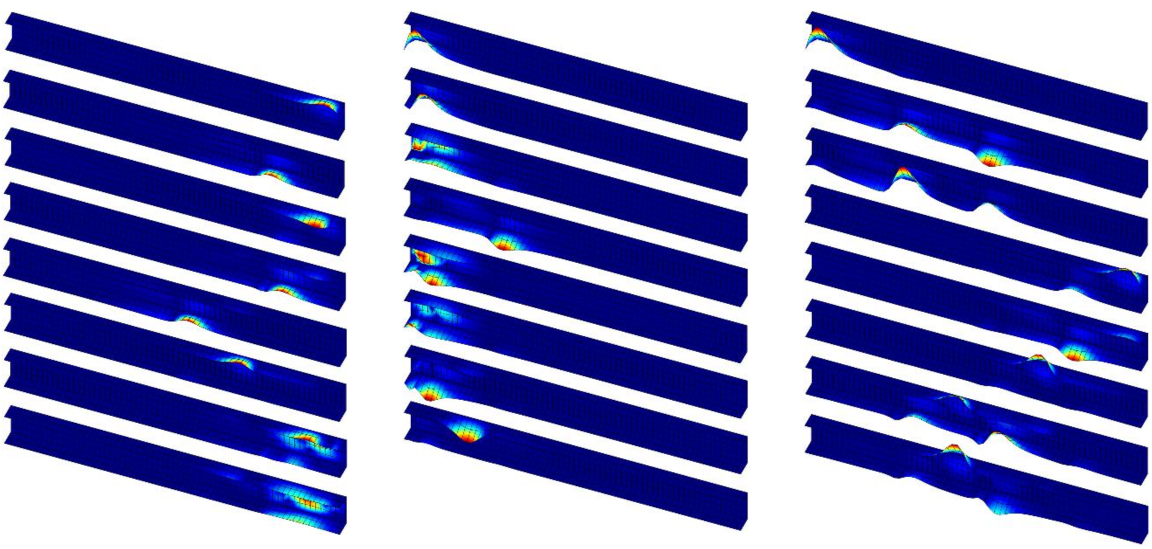

(a) Uniform thickness with 7 repeats | (b) Linear tapering from 12 to 2 repeats | (c) Linear tapering from 10 to 4 repeats

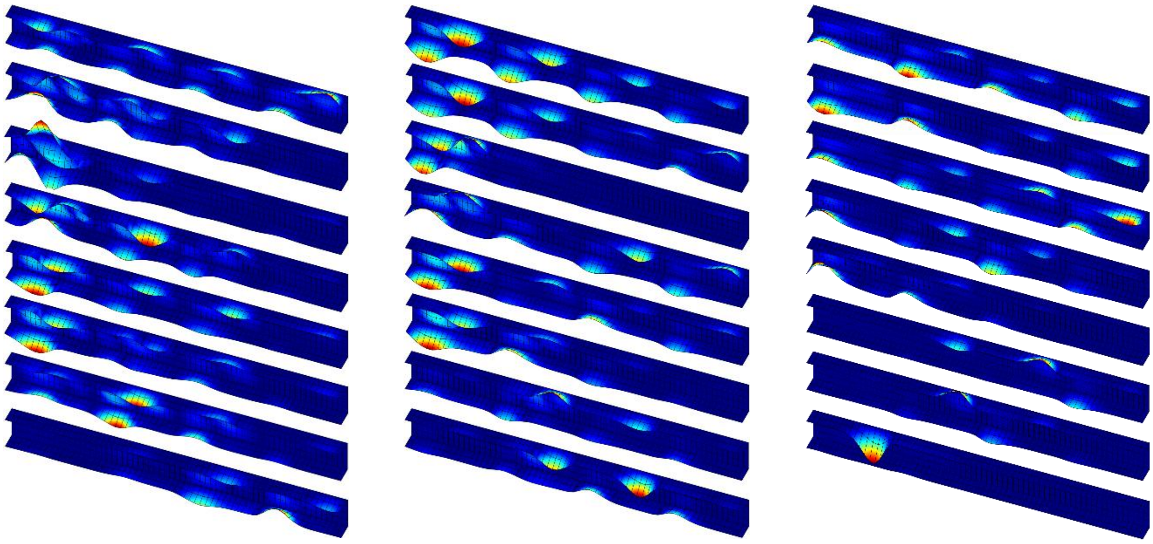

(d) Optimal tapering without spacing constraints | (e) Optimal tapering with s_{min}=31.75 mm | (f) Optimal tapering with s_{min}=95.25 mm

Figure 19. 1st to 8th buckling modes of the optimal C-spars. (The left side is the tip, and the right side is the fixed root.)

The first eight buckling modes are provided in Fig. 19 for the six different thickness profiles used in Table 5. The right side of the illustration is the fixed root. For the uniform thickness with 7 repeats in Fig. 19(a), the buckling happens around the root due to the largest vertical loading and moment at the root. For the linear thickness tapering varying from 12 to 2 repeats in Fig. 19(b), almost all the first eight buckling happens round the tip area due to the too thin thickness at this area. Combining with data in Table 5, it indicates that simple linear tapering from the upper limit of 12 repeats to the lower limit of 2 repeats not only fails to increase the critical buckling load but even leads to a significant 55.9% decrease because local buckling at the tip occurs prematurely due to the too thin thickness. Moreover, there are big increases in the buckling loads for higher buckling modes. When the thickness is tapered linearly from 10 to 4 repeats in Fig. 19(c), the first five buckling loads are close, as given in Table 5, and the buckling happens locally not only at the tip, but also at the middle or at the root. When a general thickness tapering is optimized in Figs. 19(d-f), the first seven buckling load factors are almost equal and the buckling happens simultaneously from the root to the tip and not only limited to the flange but also at the web, which indicates that the proposed optimization method tailors a general thickness variation to maximize the critical buckling load by narrowing the gaps between low-order and high-order buckling loads to achieve higher-order modes, consequently leading to a significant enhancement in the critical buckling load.

5. Conclusions

An implicit global & local modelling strategy is proposed to implement buckling optimization of DD laminates by tapering the thickness distribution. A global model with uniform thickness is used to perform buckling load calculation, while the equivalent material properties are derived from the homogenization of local DD laminates with different repeat numbers of a sub-laminate. The repeats of the sub-laminate at the nodes of the global mesh are selected as design variables to control the thickness profile. An optimization model is established to minimize the structure weight with buckling constraints or maximize the critical buckling load with the weight constraint. The thickness tapering is optimized with a gradual variation by incorporating tapering spacing constraints between adjacent thicknesses. The incorporation of spacing constraints yields a more delamination-resistant tapering profile by avoiding stress concentration due to sharp thickness variations. After that, sensitivities of the involved structural responses are calculated to facilitate the use of a high-efficient gradient algorithm.

Four typical numerical examples are presented to validate the effectiveness of the proposed method. Firstly, a benchmark problem for 18-panel horseshoe configuration is used for weight reduction. The proposed solution for the problem under local buckling constraints shows a further weight reduction comparing with literature. The problem under a global buckling constraint is investigated for soft, QI and hard stiffness and ends up to similar thickness distribution and weight reduction. Secondly, a hole-free square and a perforated square subjected to four different loading cases: uniaxial compression, biaxial compression, one shear and dual shears conclusively validate the effectiveness of the proposed method and underscore the necessity of incorporating tapering spacing constraints into the optimization process. The calculation efficiency of the proposed method is validated with about 267 times improvement compared with GA. Lastly, a larger-scale structure of a C-spar, representing an aerospace component, is used for tapering optimization for increasing buckling resistance. The optimal results reveal the significant potential of the proposed method for increasing the critical buckling load by varying the thickness profile of DD laminates in a non-uniformly loaded structure.

The optimal designs of DD laminates with a gradual thickness variation have the ability of increase the structural buckling resistance, but at the cost of increased manufacturing difficulty. These designs can be fabricated using manual operations, 3D printing and Automated Fiber placement technologies. When the performance improvement, such as buckling load increase and weight reduction, outweighs the increase in the manufacturing cost, these optimal structures will have market applications. For practical structures, especially for aerospace applications with critical lightweight requirements, the proposal methodology can be applied to generate a conceptual design by considering suitable thickness tapering spacing constraints. More manufacturing constraints can be added to the conceptual design or the further detailed design to yield manufacturing favorable structures.

Moreover, the performance improvement of laminates using the proposed method comes from the variable thickness, making it directly applicable to metal design. However, this cannot be achieved with conventional Quad laminates. DD laminates are used here for optimization because their simple and thin 4-ply sub-laminates yield constant normalized stiffness similar to metals, enabling the use of gradient-based algorithms. In contrast, Quad laminates exhibit varying normalized stiffness for single ply drops or thick sub-laminates due to the symmetric requirement and using fixed ply angles, making it difficult to apply the proposed method.

6. Acknowledgement

The IHPC authors acknowledge financial support for this research from grants (C210812010, A19C9a0044, M23L5a0002) awarded by the Agency for Science, Technology and Research (A*STAR).

References

[1] Dirk HJL, Ward C, Potter KD. The engineering aspects of automated prepreg layup: History, present and future. Composites Part B: Engineering, 2012; 43(3): 997-1009.

[2] Oromiehie E, Prusty BG, Compston P, Rajan G. Automated fibre placement based composite structures: Review on the defects, impacts and inspections techniques. Composite Structures, 2019: 224: 110987.

[3] Brasington A, Sacco C, Halbritter J, Wehbe R, Harik R. Automated fiber placement: A review of history, current technologies, and future paths forward. Composites Part C: Open Access, 2021; 6:100182.

[4] Riche RL, Haftka RT. Optimization of laminate stacking sequence for buckling load maximization by genetic algorithm. AIAA journal, 1993; 31(5): 951-956.

[5] Aymerich F, Serra M. Optimization of laminate stacking sequence for maximum buckling load using the ant colony optimization (ACO) metaheuristic. Composites Part A: Applied Science and Manufacturing, 2008; 39(2): 262-272.

[6] de Almeida FS. Stacking sequence optimization for maximum buckling load of composite plates using harmony search algorithm. Composite Structures, 2016; 143: 287-299.

[7] de Almeida FS de. Optimization of laminated composite structures using harmony search algorithm. Composite Structures, 2019; 221: 110852.

[8] Chang N, Wang W, Yang W, Wang J. Ply stacking sequence optimization of composite laminate by permutation discrete particle swarm optimization. Structural and Multidisciplinary Optimization, 2010; 41(2): 179-187.

[9] Jing Z, Fan X, Sun Q. Stacking sequence optimization of composite laminates for maximum buckling load using permutation search algorithm. Composite Structures, 2015; 121: 225-236.

[10] Ghashochi BH, Sadr M. Stacking sequence optimization of composite plates for maximum fundamental frequency using particle swarm optimization algorithm. Meccanica, 2012; 47(3): 719-730.

[11] Almeida Jr JHS, Ribeiro ML, Tita V, Amico SC. Stacking sequence optimization in composite tubes under internal pressure based on genetic algorithm accounting for progressive damage. Composite Structures, 2017; 178: 20-26.

[12] Matsuzaki R, Todoroki A. Stacking-sequence optimization using fractal branch-and-bound method for unsymmetrical laminates. Composite Structures, 2007; 78(4): 537-550.

[13] Bruyneel M, Beghin C, Craveur G, Grihon S, Sosonkina M. Stacking sequence optimization for constant stiffness laminates based on a continuous optimization approach. Structural and Multidisciplinary Optimization, 2012; 46(6): 783-794.

[14] Le-Manh T, Lee J. Stacking sequence optimization for maximum strengths of laminated composite plates using genetic algorithm and isogeometric analysis. Composite Structures, 2014; 116: 357-363.

[15] Tsai SW. Double-double: a new family of composite laminates, AIAA, 2021; 59(11):4293-305.

[16] Javidrad F, Nazari M, Javidrad HR. Optimum stacking sequence design of laminates using a hybrid PSO-SA method. Composite Structures, 2018; 185: 607-618.

[17] Zhang Z, Hou S, Liu Q, Han X. Winding orientation optimization design of composite tubes based on quasi-static and dynamic experiments. Thin-Walled Structures, 2018; 127: 425-433.

[18] Tsai SW, Sharma N, Arteiro A, Roy S, Rainsberger B. Composite double-double and grid/skin structures: low weight/low cost design and manufacturing, A Stanford/Mtorres invention, International Paris Air Show, 2019.

[19] Vermes B, Tsai SW, Massard T, Springer GS, Czigany T. Design of laminates by a novel "double–double" layup. Thin-Walled Structures, 2021; 165:107954.

[20] Kappel E. Double–Double laminates for aerospace applications—Finding best laminates for given load sets. Composites Part C: Open Access, 2022; 8: 100244.

[21] Tsai SW. Double-Double: A New Perspective in the Manufacture and Design of Composites. Composites Design Group, 2022.

[22] Gurdal Z, Olmedo R. In-plane response of laminates with spatially varying fiber orientations-variable stiffness concept. AIAA journal, 1993; 31(4): 751-758.

[23] Setoodeh S, Abdalla MM, IJsselmuiden ST, Gürdal Z. Design of variable-stiffness composite panels for maximum buckling load. Composite structures, 2009; 87(1): 109-117.

[24] Hong Z, Peeters D, Guo Y. Efficient strength optimization of variable stiffness laminates using lamination parameters with global failure index. Computers & Structures, 2022; 271: 106856.

[25] Wu Z, Raju G, Weaver PM. Framework for the buckling optimization of variable-angle tow composite plates. AIAA Journal, 2015; 53(12): 3788-3804.

[26] Kim BC, Potter K, Weaver PM. Continuous tow shearing for manufacturing variable angle tow composites. Composites Part A: Applied Science and Manufacturing, 2012; 43(8): 1347-1356.

[27] Hao P, Yuan X, Liu C, Wang B, Liu H, Li G, Niu F. An integrated framework of exact modeling, isogeometric analysis and optimization for variable-stiffness composite panels. Computer Methods in Applied Mechanics and Engineering, 2018: 339: 205-238.

[28] Xu Y, Zhu J, Wu Z, Cao Y, Zhao Y, Zhang W. A review on the design of laminated composite structures: constant and variable stiffness design and topology optimization. Advanced Composites and Hybrid Materials, 2018; 1: 460-477.

[29] Tian Y, Shi T, Xia Q. A parametric level set method for the optimization of composite structures with curvilinear fibers. Computer Methods in Applied Mechanics and Engineering, 2022; 388: 114236.

[30] Tian Y, Shi T, Xia Q. Optimization with manufacturing constraints for composite laminates reinforced by curvilinear fibers through a parametric level set method. Composite Structures, 2023; 321: 117310.

[31] Esposito L, Cutolo A, Barile M, Lecce L, Mensitieri G, Sacco E, Fraldi M. Topology optimization-guided stiffening of composites realized through automated fiber placement. Composites Part B: Engineering, 2019; 164: 309-323.

[32] Obata S, Takahashi K, Inaba K. Laminate design for a tapered FRP structure with ply drop-off based on yielding of resin pockets. Composite structures, 2020; 253: 112787.

[33] Yang J, Song B, Zhong X, Jin P. Optimal design of blended composite laminate structures using ply drop sequence. Composite Structures, 2016; 135: 30-37.

[34] Irisarri FX, Lasseigne A, Leroy FH, Le Riche R. Optimal design of laminated composite structures with ply drops using stacking sequence tables. Composite Structures, 2014; 107: 559-569.

[35] Peng X, Wang M, Yi B, Li J, Wu H, Jiang S. Optimization design of stacking sequence and material distribution for variable thickness hybrid composite structure based on improved stacking sequence table. Composite Structures, 2023; 307: 116641.

[36] Liu X, Featherston CA, Kennedy D. A novel parallel method for layup optimization of composite structures with ply drop-offs. Composite Structures, 2023; 312: 116853.

[37] Irisarri FX, Peeters DM, Abdalla MM. Optimisation of ply drop order in variable stiffness laminates. Composite Structures, 2016; 152: 791-799.

[38] Peeters DM, Irisarri FX, Groenendijk C, Růžek R. Optimal design, manufacturing and testing of non-conventional laminates. Composite Structures, 2019; 210: 29-40.

[39] Nasab FF, Geijselaers HJM, Baran I, Akkerman R, de Boer A. A level-set-based strategy for thickness optimization of blended composite structures. Composite structures, 2018; 206: 903-920.

[40] Wang D, Abdalla MM, Wang ZP, Su Z. Streamline stiffener path optimization (SSPO) for embedded stiffener layout design of non-uniform curved grid-stiffened composite (NCGC) structures. Computer Methods in Applied Mechanics and Engineering, 2019; 344: 1021-1050.

[41] Wang D, Yeo SY, Su Z, Wang ZP, Abdalla MM. Data-driven streamline stiffener path optimization (SSPO) for sparse stiffener layout design of non-uniform curved grid-

stiffened composite (NCGC) structures. Computer Methods in Applied Mechanics and Engineering, 2020; 365: 113001.

[42] Wang D, Abdalla MM, Zhang W. Sensitivity analysis for optimization design of non-uniform curved grid-stiffened composite (NCGC) structures. Composite structures 2018; 193: 224-236.

[43] Zhao W, Kapania RK. Skin-Stringer Assembly Using Radial Basis Functions for Curvilinearly Stiffened Panels. AIAA Journal, 2021; 59(3): 1125-1133.

[44] Zhao W, Singh K, Kapania RK. Thermal buckling analysis and optimization of curvilinearly stiffened plates with variable angle tow laminates. Journal of Spacecraft and Rockets, 2019; 56(4): 1189-1204.

[45] Wang Y, Wang D, Zhong Y, Rosen DW, Li S, Tsai SW. Topology optimization of Double-Double (DD) composite laminates considering stress control. Computer Methods in Applied Mechanics and Engineering, 2023; 414: 116191.

[46] Xia L, Xia Q, Huang X, Xie YM. Bi-directional evolutionary structural optimization on advanced structures and materials: a comprehensive review. Archives of Computational Methods in Engineering, 2018; 25: 437-478.

[47] Cairns DS, Mandell JF, Scott ME, Maccagnano JZ. Design and manufacturing considerations for ply drops in composite structures. Composites Part B: Engineering, 1999; 30(5): 523-534.

[48] Mukherjee A, Varughese B. Design guidelines for ply drop-off in laminated composite structures. Composites Part B: Engineering, 2001; 32(2): 153-164.

[49] Gordon T, Wisnom MR, Kim BC. Suppression of compression induced delamination in tapered laminated composites using a ply scarfing method. Composites Part A: Applied Science and Manufacturing, 2024; 176: 107870.

[50] Gordon T, Xu X, Wisnom MR, Hallett SR, Kim BC. Improved impact damage resistance of tapered composite laminates using a ply scarfing technique. Composites Part A: Applied Science and Manufacturing, 2023; 166: 107391.

[51] Peeters D, Deane M, Higgins O'R, Weaver PM. Morphology of ply drops in thermoplastic composite materials manufactured using laser-assisted tape placement. Composite Structures, 2020; 251: 112638.

[52] Damghani, M., Matthews, J., Murphy, A. and Featherston, C., 2023, May. Numerical shape, thickness and stacking sequence optimisation and experimental study of hybrid composite plates under in-plane shear loading. In Structures (Vol. 51, pp. 372-390). Elsevier.

[53] Svanberg K. A class of globally convergent optimization methods based on conservative convex separable approximations, SIAM journal on optimization 2002; 12 (2): 555–573.

[54] Soremekun G, Gürdal Z, Kassapoglou C, Toni D. Stacking sequence blending of multiple composite laminates using genetic algorithms. Composite structures, 2002; 56(1): 53-62.

[55] IJsselmuiden ST, Abdalla MM, Seresta O, Gürdal Z. Multi-step blended stacking sequence design of panel assemblies with buckling constraints. Composites part B: engineering, 2009; 40(4): 329-336.